SCIENTIFIC REPORTS

OPEN

SUBJECT AREAS:
COORDINATION CHEMISTRY
MAGNETIC MATERIALS

Received
18 March 2014

Accepted
29 May 2014

Published
27 June 2014

Correspondence and requests for materials should be addressed to J.T. (tang@ciac.ac.cn); L.F.C. (Liviu.Chibotaru@chem.kuleuven.be) or D.C. (dmcui@ciac.ac.cn)

An NCN-pincer ligand dysprosium single-ion magnet showing magnetic relaxation *via* the second excited state

Yun-Nan Guo[1,3], Liviu Ungur[4], Garrett E. Granroth[5], Annie K. Powell[6], Chunji Wu[2], Stephen E. Nagler[5], Jinkui Tang[1], Liviu F. Chibotaru[4] & Dongmei Cui[2]

[1]State Key Laboratory of Rare Earth Resource Utilization, Changchun Institute of Applied Chemistry, Chinese Academy of Sciences, Changchun 130022, P. R. China, [2]State Key Laboratory of Polymer Physics and Chemistry, Changchun Institute of Applied Chemistry, Chinese Academy of Sciences, Changchun 130022, P. R. China, [3]School of Science, Xi'an Jiaotong University, Xi'an 710049, P. R. China, [4]Theory of Nanomaterials Group, Department of Chemistry, Katholieke Universiteit Leuven, Celestijnenlaan 200F, 3001 Leuven, Belgium, [5]Oak Ridge National Laboratory, Oak Ridge, Tennessee 37831, USA, [6]Institute of Inorganic Chemistry, Karlsruhe Institute of Technology, Engesserstrasse 15, 76131 Karlsruhe, Germany and Institute of Nanotechnology, Karlsruhe Institute of Technology, Hermann-von-Helmholtz-Platz 1, Eggensteinn-Leopoldshafen, 76344 Karlsruhe, Germany.

Single-molecule magnets are compounds that exhibit magnetic bistability purely of molecular origin. The control of anisotropy and suppression of quantum tunneling to obtain a comprehensive picture of the relaxation pathway manifold, is of utmost importance with the ultimate goal of slowing the relaxation dynamics within single-molecule magnets to facilitate their potential applications. Combined *ab initio* calculations and detailed magnetization dynamics studies reveal the unprecedented relaxation mediated *via* the second excited state within a new DyNCN system comprising a valence-localized carbon coordinated to a single dysprosium(III) ion. The essentially C_{2v} symmetry of the Dy^{III} ion results in a new relaxation mechanism, hitherto unknown for mononuclear Dy^{III} complexes, opening new perspectives for means of enhancing the anisotropy contribution to the spin-relaxation barrier.

Acting as a tiny magnets, Single-molecule magnets (SMMs)[1] are chemically and physically interesting compounds as a platform on which to build future spin-based devices[2–7]. Recently the enormous potential of lanthanide(III) ions[8], and dysprosium in particular[9–13], has been recognized as a potential source of both the high spin and high anisotropy required for SMM behavior[14,15]. The blocking of magnetization for Ln-SMMs arises as a result of strong axiality of ground state, which for ions with odd number of electrons (e.g., Dy^{III}) implies the transversal components g_x, g_y be dwarfed by axial components g_z[16–22]. The spin is then forced to undergo reversal through a thermally activated process giving a relaxation which follows an Arrhenius behavior with a barrier Δ. This can be likened to a *levee* that prevents flooding by water even if one side of the levee is lower than the other (Figure 1). For the barrier of the levee in Louisiana, conforming to the laws of classical physics, the water is not breaking through rather than having to go over the top of the barrier. For a SMM, which is an quantum object, it is a question whether the spins can tunnel (break) through the barrier or can be forced to overcome the barrier.

Breaking through such a *levee* for a SMM is always constrained by the separation between the bistable ground state and the first excited state[23] and arises from the removing the $(2J + 1)$-fold degeneracy of the ground multiplet provided by the surrounding crystal field (Figure 1, left). The implication to enhance SMM behavior is that we can construct a high *levee* by elaborating the coordination environment of the lanthanide ions to give suitable constraints to tunneling processes (Figure 1, right). In previous *ab initio* studies, this scenario was explored by considering an idealized diatomic $[DyO]^+$ complex[21]. As a result of the perfect axiality of all of the Kramers doublets (KDs) the transversal magnetic field induces a tunneling splitting in $[DyO]^+$ only at the highest order of perturbation theory, following a path similar to that of the reversed double-well potential of Mn_{12}-Ac[24]. The difference is that, for Ln^{III} ions, the total multiplet width of CF splittings of the order of 100–1000 cm^{-1} open huge perspectives for means of enhancing the anisotropy contribution to the magnetic relaxation barrier.

So far a clear-cut example of such a magnetic relaxation *via* higher excited state energy levels has never been seen before for Ln complexes. Here, we chose to probe the magnetism of a localized Dy-C bond

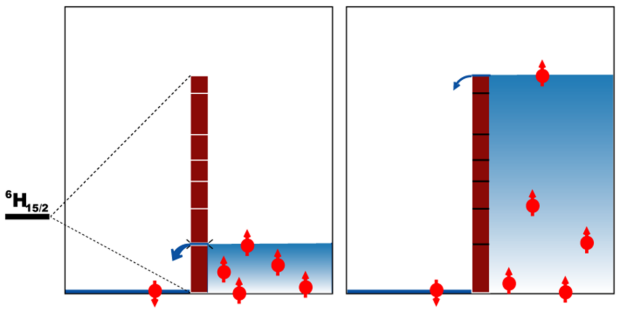

Figure 1 | Barrier *levee* model for design Ln-SMMs. With Dy^{III} for example, where the magnetic moment is forced to undergo reversal through a thermally activated process. (Left) Magnetization reversal constrained by the first excited state; (Right) Magnetization reversal forced to the highest excited state.

containing complex stabilized by an aryldiimino NCN-pincer ligand (Inset of Figure 2), as exists in [2,6-(2,6-$C_6H_3R_2N{=}CH)_2$-C_6H_3]-$DyCl_2(THF)_2$ (DyNCN). More striking still, this unique Dy-C bond occupies the crystallographic C_2 axis in DyNCN. The combination of *ab initio* calculations and detailed magnetization dynamics studies reveals the two lowest Kramers doublets being extremely axial in nature and possessing parallel anisotropy axes along C_2 direction, which results in the unprecedented relaxation going *via* the second excited state in compound DyNCN.

Results and discussion

X-Ray structure analysis. Compound DyNCN was synthesized *via* transmetalation between 2,6-(2,6-$C_6H_3R_2N{=}CH)_2$-C_6H_3Li and $LnCl_3(THF)_{1\sim3.5}$[25], and crystallizes in the space group $P4_32_12$, with $Z = 4$. The whole molecule exhibits C_2 crystallographic symmetry, in which the Dy–C bond is located on a 2-fold rotation axis $[\frac{\sqrt{2}}{2}\frac{\sqrt{2}}{2}0]$. The monoanionic NCN-pincer ligand coordinates to the central metal ion in a κC: κN: κN' tridentate mode to form a meridional conformation. The two N-aryl rings dispose the vertical positions against the NCN plane, which are parallel to the two *cis*-located THF rings, respectively. The chloride groups arrange in *trans*-positions to

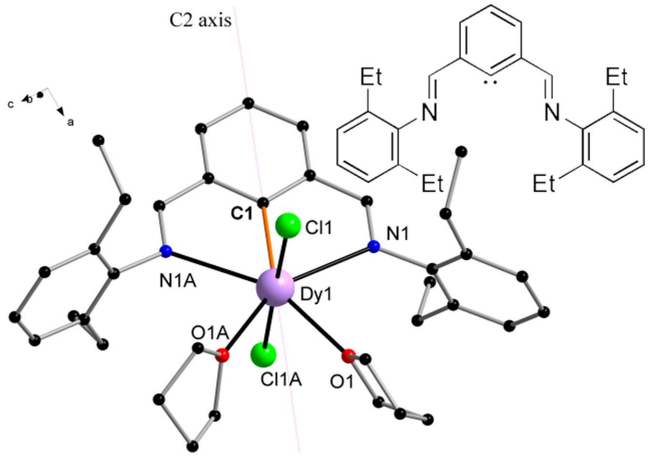

Figure 2 | Molecular structure. Structure of [2,6-(2,6-$C_6H_3R_2N{=}CH)_2$-C_6H_3]-$DyCl_2(THF)_2$ (DyNCN) molecule with the Dy-C bond highlighted in orange. Blue, Dy; green, Cl; black, C; blue, N; red, O. H atoms and a THF solvent molecule are omitted for clarity. Complex LuNCN exhibits analogous structure. Coordination bond distances (Å) for DyNCN: Dy-C = 2.3933(25), Dy-Cl = 2.5960(8), Dy-N = 2.6689(24) and Dy-O = 2.4484(20). Inset: The structure of the NCN-pincer ligand [2,6-(2,6-$C_6H_3Et_2N{=}CH)_2$-C_6H_3]$^-$.

form a large Cl–Dy–Cl angle (176.500(23)°) bisected by the NCN plane. Therefore, if one focuses only on the atoms of the first coordination sphere two nearly exactly perpendicular planes (C1/N1/O1/O1A/N1A) and (C1/Cl1/Cl1A) are formed. Then the effective CF is of C_{2v} symmetry.

Electronic structure calculations. The interaction of the 4f orbitals involved in the formation of the robust organometallic surroundings seems to play a key role in the LF thereby enhancing the magnetic properties. A few carbon ring coordinated Ln-based SMMs, that include ligands such as cyclopentadienide and cyclooctatetraenide, have generated profound thoughts and enlightenment[22,26–30]. The discovery of these bona fide organometallic SMMs underscores the significance of making use of the simple Ln-C bond to design molecules with strong axiality[31]. The title compound with a strong single Dy–C bond combining the huge conjugation effect of a carbanion offers a new paradigm for single ion anisotropy as shown from the *ab initio* calculated electronic structure of lowest eight Kramers doublets of DyNCN in Table 1 (see Experimental Section and the ESI of Figure S1–S7 and Table S1–S8 for details).

Table 1 shows the low lying spin-orbit energy spectrum of the DyNCN molecule in the largest computational model. We notice a large energy separation of the ground and first exctied Kramers doublets. As shown in Figure 3, the main anisotropy axis of the complex passes along the main symmetry axis of the complex, i.e. it is parallel to the Dy-C chemical bond. The reason for the strong effect of the ligating C atom is the fact that it holds a negative charge as the ligand is a carbanion. The calculated Mulliken charge on the carbon atom revealed a negative charge of −1.17 on the ligating carbon atom. The localized character of the negative charge is probably due to intramolecular electrostatic effects: the negative charge of the carbanion is attracted by positively charged Dy^{III} ion, and the ligating C atom is the closest point to the Dy^{III} ion. This is also the reason why the Dy-C bond is unusually short (≈2.39 Å). Even though the computed Mulliken charges on both chlorine atoms are slightly larger (−1.60), the longer Dy-Cl distances (≈2.60 Å) make the cumulative (total) effect of both chlorine atoms less important for the magnetic anisotropy of the two low lying Kramers doublets than the influence of the much closer carbon atom. In fact, we have already seen for other complexes that the main anisotropy axis is mainly oriented by the effect of the closest ligand[21].

As a result of the above described effects, we notice an interesting fact of *collinearity* of the main anisotropy axes in the ground (almost pure ±15/2) and first excited (almost pure ±13/2) doublets. We will see later that, the collinearity of anisotropy axes is a key factor for enhancing the magnetic blocking performance of this compound.

Analysing further the magnetic anisotropy of the second excited KD (262 cm^{-1}) we notice that it is again very axial, i.e. of ±15/2 type, but its main magnetic axis is perpendicular to the main symmetry axis of the complex, passing through the two chlorine atoms. The third, fourth and fifth excited KDs are less axial, while the sixth and seventh excited KDs are again highly axial, with their main

Table 1 | *Ab initio* calculated energies of low-lying Kramers doublets in DyNCN (187 K structure) in units of cm^{-1}

Free-Ion Multiplet	Energy (cm^{-1})	g_X	g_Y	g_Z
$^6H_{15/2}$	0	9.69E-04	2.12E-03	19.8101
	176	8.72E-03	3.46E-02	17.0586
	262	0.4261	0.4374	19.4439
	348	1.9619	2.5423	12.8581
	445	8.0980	7.2355	5.4345
	526	0.4681	0.6001	14.0454
	597	0.5562	0.6565	19.4099
	645	5.87E-02	0.2346	19.3829

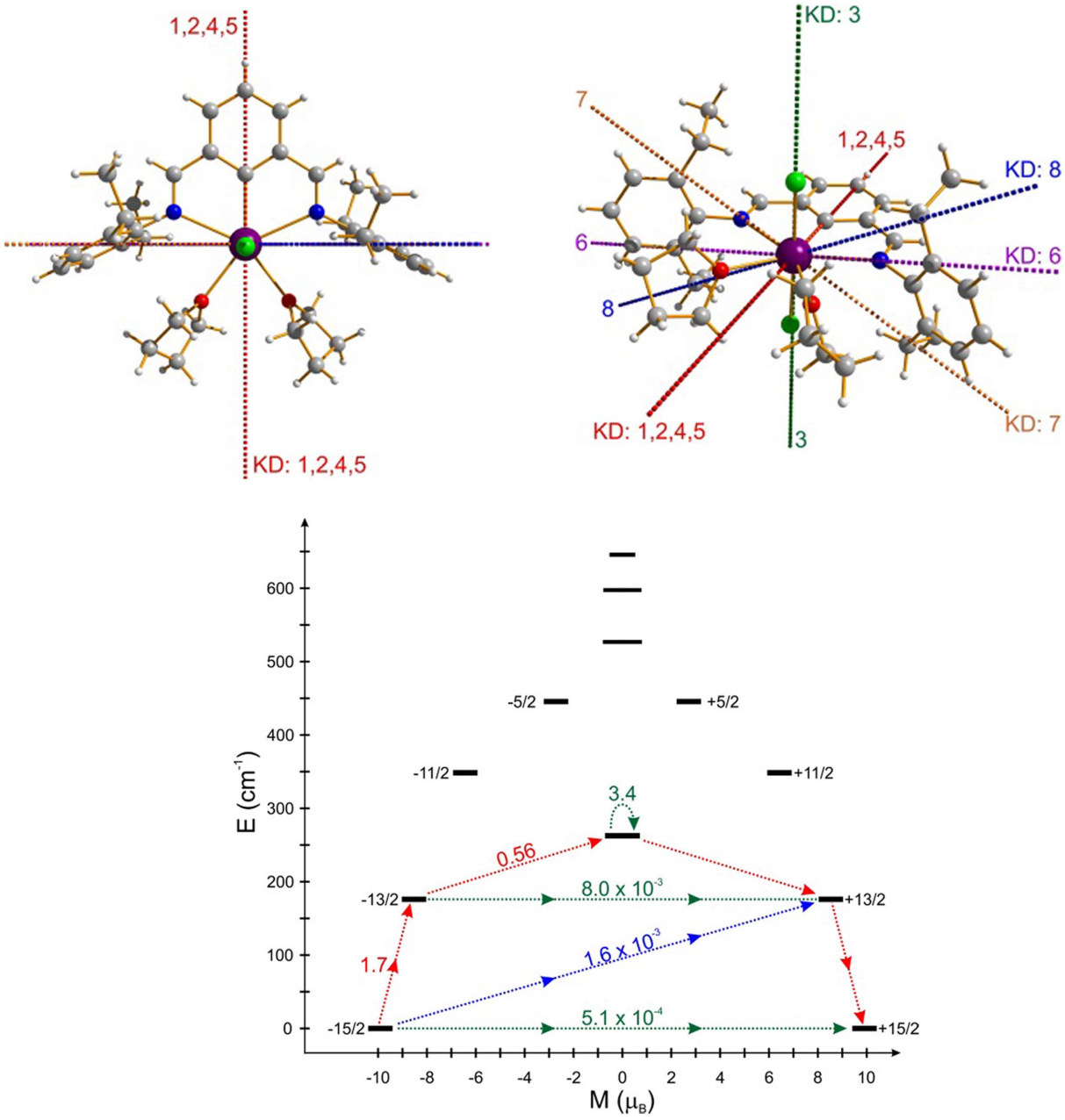

Figure 3 | Low-lying electronic structure for DyNCN. (Top) Anisotropy axes in eight lowest Kramers doublets at the Dy site of DyNCN (KD: 1–8 ranked in order of the energy from ground state to the seventh excited state as shown in below scheme). The red dashed line corresponds to the anisotropy axis of KD: 1, 2, 4 and 5; the green dashed line shows the anisotropy axis of the second excited KD (KD 3 lying at 262 cm^{-1}). (**Bottom**) Magnetization blocking barrier of the DyNCN. The black lines represent the energy levels of the ground multiplet $J = 15/2$ aligned according their magnetic moment on the C_2 symmetry axis. The arrows represent the averaged matrix element of the transversal magnetic moment connecting the corresponding states, given as $(|\mu_x| + |\mu_y| + |\mu_z|)/3$. The red arrows show the most probable path for the magnetic relaxation at high temperatures.

anisotropy axis lying in the plane perpendicular to the main symmetry axis of the complex[21].

Table 2 shows the parameters of the crystal field acting on the ground atomic multiplet $J = 15/2$ of the Dy^{III} ion. We notice that, although the *ab initio* calculation was performed in the C_1 point group (i.e. effectively ignoring the symmetry) the departure from the perfect point group symmetry is very small, leading to the fact that only parameters of the even projection on the quantization axis enter in the decomposition of the *ab initio* energy matrix. The largest parameter, B_2^0 sets the main anisotropy axis of the ground and of the first excited KD, while the significant value of the second largest parameter, B_2^2, is probably responsible for the anisotropy of the second excited KD. In other words, the B_2^2 parameter is the largest in the case when the quantization axis is parallel to the main anisotropy axis of the second excited KD, i.e. passing along the Cl-Cl axis.

The *ab initio* calculated magnetic properties of DyNCN are in good agreement with direct current (dc) magnetic susceptibility measurements (Figure S7) which gives confidence in the anisotropic properties of the low-lying KDs discussed above. In addition, as shown in Figure S8, the preliminary powder INS spectra obtained on DyNCN exhibit two peaks, around 19 and 28 meV, that are also roughly consistent with the state transitions predicted by the *ab initio* calculation. Unfortunately the strong H background prevents a more detailed statement on the level structure and further investigations will be discussed in a separate publication.

Table 2 | *Ab initio* calculated parameters of the crystal field acting on the ground $J = 15/2$ multiplet on the basis of the *ab intio* results presented in Table 1 (in units of cm^{-1}). The parameters are given for the coordinate system employed in the *ab initio* calculations (given in the SI)

k	q	parameters of the crystal field B_k^q
2	−2	−0.8223285E + 00
2	0	−0.2952967E + 01
2	2	0.2085183E + 01
4	−4	0.5765483E − 02
4	−2	−0.9592991E − 03
4	0	−0.4952142E − 02
4	2	−0.2436407E − 01
4	4	−0.3230413E − 01
6	−6	0.3422329E − 04
6	−4	0.1810159E − 04
6	−2	0.4855725E − 04
6	0	0.2270114E − 04
6	2	−0.1666892E − 04
6	4	0.6830792E − 04
6	6	−0.6617125E − 04

Static magnetic properties. The investigation of the magnetic properties of a polycrystalline sample revealed a room temperature $\chi_M T$ value of 13.8 cm^3 K mol^{-1} (Figure S7), in agreement with the expected value for $g = 4/3$ of the $^6H_{15/2}$ ground state of a single Dy^{III}. A gradual decrease on lowering the temperature is observed above 10 K and attributed to the depopulation of the substates. The lowest Kramers doublet has strong uniaxial magnetic anisotropy along the C_2 axis. The next Kramers doublet lies at about 176 cm^{-1}. The large energy difference results in a predominant population of the lowest levels up to relatively high temperature: the population ratio remains 99.3% at 50 K. Thus, the static magnetic behavior of the complex below 50 K is almost exclusively described by the ground doublet.

Dynamic magnetic properties. However, dynamic magnetic properties will be strongly influenced by the nature of excited substates. To investigate this possibility, variable-frequency alternating current (ac) magnetic susceptibility measurements were performed.

As the hallmark of a SMM, the in-phase (χ') and out-of-phase (χ'') component, of DyNCN are characterized by the frequency dependence below ~35 K going through a frequency dependent maximum (>100 Hz) on lowering the temperature (Figure 4a, b), signaling the "freezing" of the spins by the anisotropy barrier arising from the split substates. To quantify the thermally activated process, the χ'' curves were divided by the dc susceptibility χ_{dc}, in which the relaxation time τ matches the inverse of the angular frequency $2\pi\nu$ exactly at the peak temperature of the corresponding curve (Figure S9)[32,33]. As expected for a single-molecule magnet, the relaxation times exhibit an exponential dependence on temperature between 24 and 27.5 K, and an Arrhenius fit to the data gives an effective relaxation barrier of U_{eff} = 233(4) cm^{-1}, with a pre-exponential factor of $\tau_0 = 6(1) \times 10^{-10}$ s (Figure 5). The barrier height of DyNCN is more than 50 cm^{-1} above the first excited KD, which strongly supports the assignment that an Orbach process occurs through the second excited state (Figure 3 Bottom). This assignment is consistent with *ab initio* calculated energy of the second excited KD (266 cm^{-1} in the best approximation (see the ESI)), which fits perfectly the barrier U_{eff} = 270(5) cm^{-1} extracted for the diluted sample (Figure 5).

On cooling, deviations from the Arrhenius law become more and more important, which indicates that the blocking under this barrier is not complete and not even observable at all when $T < 10$ K with a temperature-independent relaxation time 10^{-4} s. The observed relaxation rate at this temeprature is entirely due to quantum tunneling of magnetization (QTM). In the undiluted sample of DyNCN the QTM is mainly due to the contribution of magnetic dipolar interactions to the transversal component of internal magnetic field H_{dip} at each Dy site. This leads to the tunneling splitting of the ground-state Kramers doublet by the amount $\Delta_{tun} = g_{X,Y}\mu_B H_{dip}$, while this tunneling gap contributes directly to the QTM relaxation rate. Given the relatively large value of the latter (Figure 5a), magnetic hysteresis in this compound is only observed without coercivity using the sweep rate accessible with a conventional magnetometer (Figure 6).

In order to reduce the influence of the molecular surrounding on the spin dynamics of the dysprosium ion, magnetic measurements on a sample in which Dy^{III} is magnetically diluted by the isostructural Lu^{III} analogue in a molar ratio of 1 : 19 ($Dy_{0.05}Lu_{0.95}NCN$) were performed. In contrast to the pure DyNCN, hysteresis is observed with a small coercive field for the diluted sample (inset of Figure 6). As a result of reduction of thansversal component of internal field H_{dip} upon dilution, the relaxation times at low temperatures are two orders of magnitude slower than those operating in the undiluted sample. Therefore, as observed also in other crystals containing SMMs[34], magnetic site dilution effectively chokes the pathway for ground state quantum tunneling. Here, the ac spectra could only be recorded only within a limited frequency range of 0.04 Hz, which prevented observation of the more sluggish real quantum regime at temperatures below 6 K.

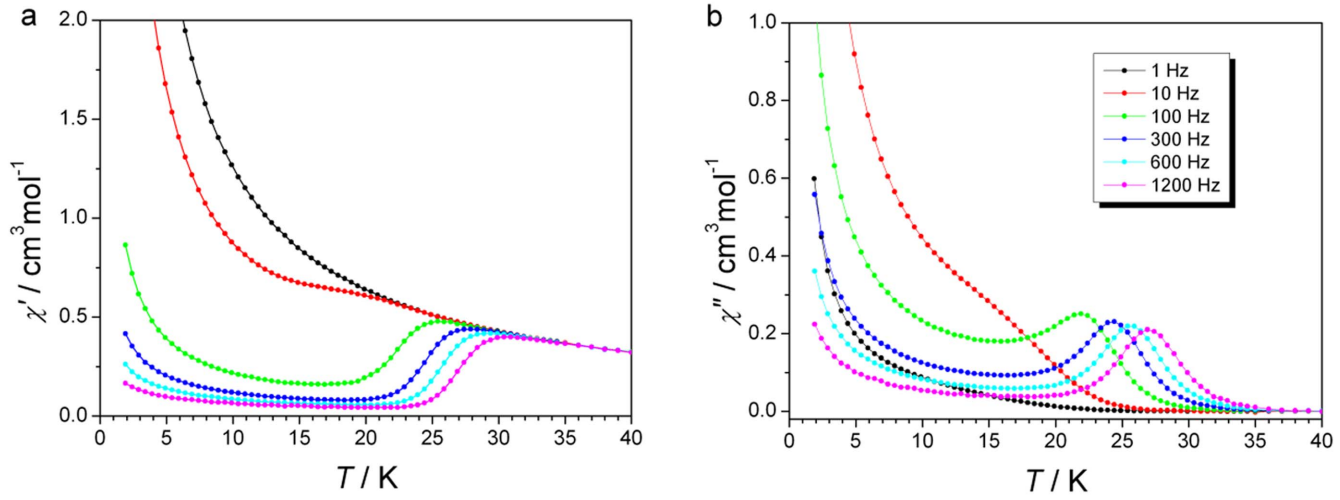

Figure 4 | ac susceptibility. Temperature dependence of the in-phase (χ', a) and out-of-phase (χ'', b) components of the ac magnetic susceptibility for DyNCN under zero applied dc field.

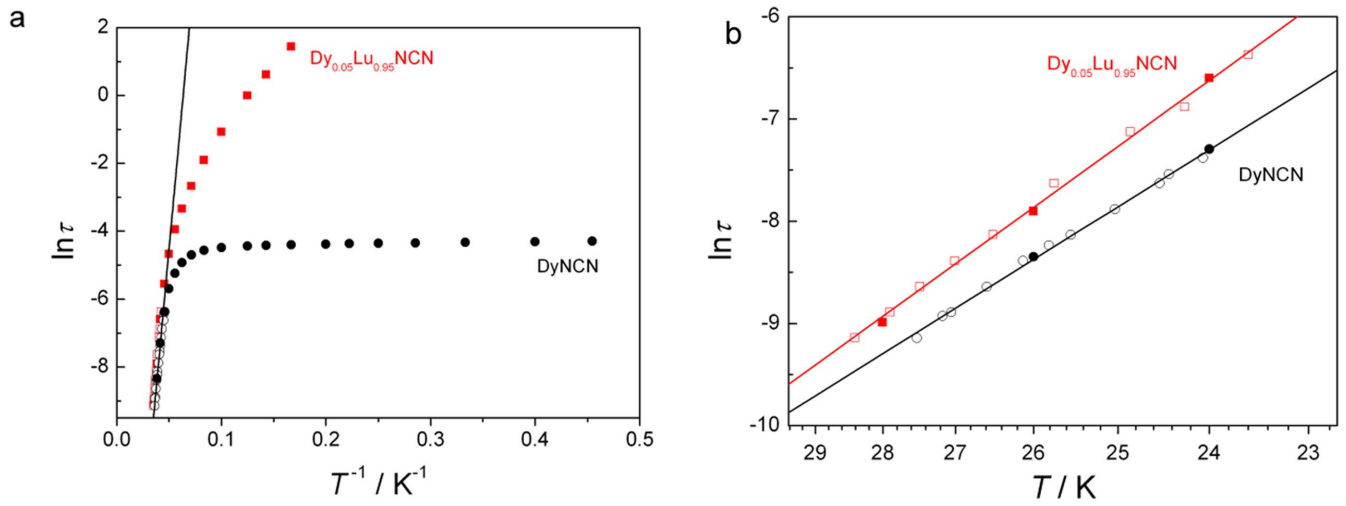

Figure 5 | Relaxation times. (a) Plot of inverse temperature versus the natural log of the relaxation time for DyNCN (black circle) and $Dy_{0.05}Lu_{0.95}NCN$ (red square). In the higher temperature part shown as hollow symbols, relaxation times are extracted from χ''/χ_{dc} (T) diagrams (Figure S9); relaxation times represented by solid symbols are determined from χ'' (ν) diagrams (Figure S10). (b) Highlight of Arrhenius plots at high-temperature regime in Figure 5a. The solid lines correspond to a fit to the Arrhenius low for DyNCN and $Dy_{0.05}Lu_{0.95}NCN$, respectively, affording U_{eff} (DyNCN) = 233(4) cm^{-1} and U_{eff} ($Dy_{0.05}Lu_{0.95}NCN$) = 270(5) cm^{-1}.

Figure S11 shows that in the presence of an external dc field H the relaxation rate τ^{-1} increses in the pure DyNCN compound and decreases in the diluted $Dy_{0.05}Lu_{0.95}NCN$ sample. The applied magnetic field is known to suppress the QTM and to enhance the direct relaxation process. We may conclude from Figure S11 that the variation of the two contributions do not cancel each other completely, so that the total relaxation rate increases in the former and decreases in the second compound with applied magnetic field.

Upon increasing the temperature to the thermally activated regime (23.6–28.4 K), the relaxation time is hardly affected by magnetic dilution, and from this we can extract the slightly larger energy barrier of U_{eff} = 270(5) cm^{-1} ($\tau_0 = 1.3(3) \times 10^{-10}$ s) which comes closer to the value expected from the height of the second excited Kramers doublet.

The relaxation *via* the second excited state in the compounds DyNCN and $Dy_{0.05}Lu_{0.95}NCN$ (Figure 3 bottom), jointly confirmed by ac susceptibility and *ab initio* calculation, is remarkable and totally unprecedented since it originates from a C_2 symmetry of the complex. Contrary to what is reported here, the relaxation *via* the second excited state, recently observed on some Dy sites of K_2Dy_4 and Dy_5 complexes[34], is achieved due to very strong Dy-O interaction with one of the oxygen ions and not due to symmetry reasons. Furthermore, the obtained results further allow us to support the use of the CASSCF/RASSI-SO method as a suitable tool for the determination of strength of Ln crystal field in lanthanide-based molecules, especially, to be able ultimately to elaborate the crystal field splitting for the systems with low symmetry coordination environments.

Conclusions

In summary, a new carbon coordinated dysprosium single ion magnet, DyNCN, in which the Dy^{III} ion possesses an effective C_{2v} crystal field symmetry has been investigated. The presence of the C_2 symmetry axis requires that several low-lying KDs of the magnetic anisotropy axes coincide with it, as corroborated by *ab initio* calculations resulting in the two lowest Kramers doublets being strongly axial and possessing parallel anisotropy axes. This explains the observed thermally activated relaxation *via* the second excited KD. This new relaxation mechanism, offers a means to exploit single ion effects of lanthanide possessing perfect axial symmetry in order to facilitate magnetic relaxation climbing up to a higher energy levels, and to further open up a broader space for enhancing the anisotropy barrier. Furthermore, our findings should stimulate interest for the synthesis and characterization of organometallic lanthanide-based compounds.

Methods

Synthesis. The synthesis of the compound DyNCN and the Lu analogue are described in literature[25].

Magnetic measurements. Magnetic susceptibility measurements were performed in the temperature range 2–300 K, using a Quantum Design MPMS XL-7 SQUID magnetometer equipped with a 7 T magnet. The dc measurements were collected from 2 to 300 K and the ac measurements were carried out in a 3.0 Oe ac field oscillating at various frequencies from 1 to 1500 Hz and with a zero dc field. The diamagnetic corrections for the compounds were estimated using Pascal's constants[35], and magnetic data were corrected for diamagnetic contributions of the sample holder.

Inelastic neutron scattering. The neutron spectroscopy measurements were performed on the SEQUOIA spectrometer[36,37] at the Spallation Neutron Source of

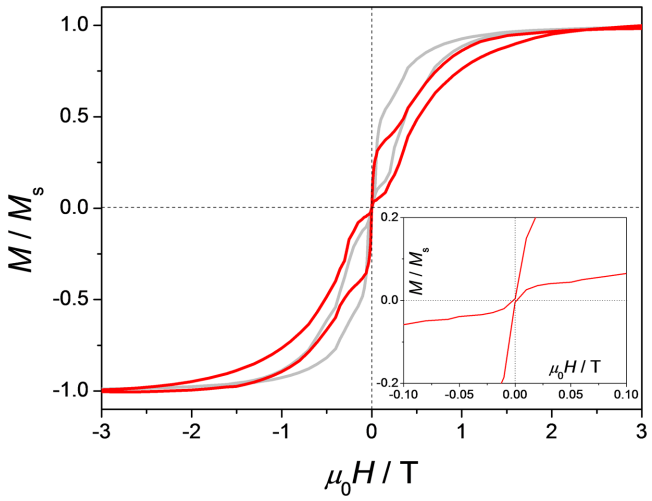

Figure 6 | Magnetic hysteresis. Magnetic hysteresis at 1.9 K at a sweep rate accessible with a conventional magnetometer for DyNCN (grey) and $Dy_{0.05}Lu_{0.95}NCN$ (red) with a clear opening of the hysteresis curves. Inset: A small coercive field of hysteresis observed in $Dy_{0.05}Lu_{0.95}NCN$.

Oak Ridge National Laboratory. The coarse resolution chopper was phased for and incident energy of 70 meV and spun at 240 Hz. A 1.71 g sample was sealed in an He atmosphere in a flat clan to fully cover the 5 cm × 5 cm beam. The sample was designed to minimize the amount of time needed to see a signal above the H background. The sample was cooled to ~5 K using a closed cycle He refrigerator. The raw time of flight data were converted to instrument independent units of Q and energy transfer and is normalized by V to remove detector efficiency differences.

***Ab initio* calculations.** All *ab initio* calculations were performed with the Molcas 7.8 *ab initio* quantum chemistry program package[38]. All *ab initio* calculations were performed on the experimental X-ray structure, without employing optimization of the molecular structure by computational methods.

All elements were described using standard relativistic basis sets from the ANO-RCC library available in Molcas[39]. Several basis set models were employed in order to test the stability of the obtained solutions. Contractions of the employed basis sets for each atom for all computational models are given in the ESI. The results presented further in the main text correspond to the largest basis set model. In this model the Dy, Cl, N, O and C from the first coordination sphere were described by a QZP basis set, TZP quality basis sets were assigned for the atoms from the second coordination sphere, while the remaining atoms were described by DZP quality basis set. In order to save disk space, the Cholesky decomposition of bielectronic integrals was employed with a threshold of 0.5×10^{-7}.

The spin eigenstates were calculated within the Complete Active Space Self-Consistent Field (CASSCF) method[40]. The active space of the CASSCF method included 9 electrons of Dy^{III} spanning seven 4f-type orbitals. The [2,6-(2,6-$C_6H_3R_2N$ =CH)$_2$-C_6H_3] carbanion is a closed shell molecule, and the HOMO does not enter into the active space. This was confirmed from test calculations on a smaller fragment (ESI) including the HOMO orbital of the carbanion into the active space which showed that this does not influence the overall results. The spin-orbit coupling was taken into account within the restricted active space state interaction (RASSI) method[41], by mixing all 21 spin-sextet states (corresponding to the free ion multiplets ^{6}H, ^{6}F and ^{6}P), 128 spin quartet states (^{4}I, ^{4}F, ^{4}M, ^{4}G, ^{4}K, ^{4}L, ^{4}D, ^{4}H, ^{4}P ^{4}G, ^{4}F, and ^{4}I), and 130 spin-doublet states (^{2}L, ^{2}K, ^{2}P, ^{2}N, ^{2}F, ^{2}M, ^{2}H, ^{2}D, ^{2}G and ^{2}O). On the basis of the resulting spin-orbital multiplets, the SINGLE_ANISO[42] program was used to compute Zeeman splitting (*g* tensor) and static magnetic properties, molar magnetic susceptibilty and magnetization. Furthermore, a recent development allows, within the SINGLE_ANISO module, for a one-to-one mapping of the *ab initio* results onto the classical crystal field acting on the ground $J = 15/2$ multiplet. In other words, the reported crystal field parameters (Eq. 1) for the investigated DyNCN compound are obtained by a direct projection of the *ab intio* results and not by fitting.

The employed CF Hamiltonian is:

$$H_{CF} = \sum_{k,q} B_k^q O_k^q \qquad (1)$$

where B_k^q are the parameters describing the crystal field, while O_k^q are the Extended Stevens Operators[43].

Furthermore, on the basis of the obtained results, the structure of the blocking barrier was analysed.

1. Gatteschi, D., Sessoli, R. & Villain, J. *Molecular Nanomagnets* (Oxford University Press, 2006).
2. Gatteschi, D., Caneschi, A., Pardi, L. & Sessoli, R. Large clusters of metal-ions - the transition from molecular to bulk magnets. *Science* **265**, 1054–1058 (1994).
3. Sessoli, R. *et al.* High-spin molecules: $[Mn_{12}O_{12}(O_2CR)_{16}(H_2O)_4]$. *J. Am. Chem Soc.* **115**, 1804–1816 (1993).
4. Leuenberger, M. N. & Loss, D. Quantum computing in molecular magnets. *Nature* **410**, 789–793 (2001).
5. Hill, S., Edwards, R. S., Aliaga-Alcalde, N. & Christou, G. Quantum coherence in an exchange-coupled dimer of single-molecule magnets. *Science* **302**, 1015–1018 (2003).
6. Bogani, L. & Wernsdorfer, W. Molecular spintronics using single-molecule magnets. *Nat. Mater.* **7**, 179–186 (2008).
7. Urdampilleta, M., Klyatskaya, S., Cleuziou, J. P., Ruben, M. & Wernsdorfer, W. Supramolecular spin valves. *Nat. Mater.* **10**, 502–506 (2011).
8. Sessoli, R. & Powell, A. K. Strategies towards single molecule magnets based on lanthanide ions. *Coord. Chem. Rev.* **253**, 2328–2341 (2009).
9. Gatteschi, D. Anisotropic dysprosium. *Nat. Chem.* **3**, 830–830 (2011).
10. Guo, Y.-N., Xu, G.-F., Guo, Y. & Tang, J. Relaxation dynamics of dysprosium(III) single molecule magnets. *Dalton Trans.* **40**, 9953–9963 (2011).
11. Blagg, R. J., Muryn, C. A., McInnes, E. J. L., Tuna, F. & Winpenny, R. E. P. Single pyramid magnets: Dy_5 pyramids with slow magnetic relaxation to 40 K. *Angew. Chem. Int. Ed.* **50**, 6530–6533 (2011).
12. Chibotaru, L. F., Ungur, L. & Soncini, A. The origin of nonmagnetic Kramers doublets in the ground state of dysprosium triangles: Evidence for a toroidal magnetic moment. *Angew. Chem. Int. Ed.* **47**, 4126–4129 (2008).
13. Rinehart, J. D., Fang, M., Evans, W. J. & Long, J. R. Strong exchange and magnetic blocking in N_2^{3-}-radical-bridged lanthanide complexes. *Nat. Chem.* **3**, 538–542 (2011).
14. Woodruff, D. N., Winpenny, R. E. P. & Layfield, R. A. Lanthanide Single-Molecule Magnets. *Chem. Rev.* **113**, 5110–5148 (2013).
15. Cucinotta, G. *et al.* Magnetic anisotropy in a dysprosium/DOTA single-molecule magnet: Beyond simple magneto-structural correlations. *Angew. Chem. Int. Ed.* **51**, 1606–1610 (2012).
16. Lin, P. H. *et al.* A polynuclear lanthanide single-molecule magnet with a record anisotropic barrier. *Angew. Chem. Int. Ed.* **48**, 9489–9492 (2009).
17. Feltham, H. L. C. *et al.* A non-sandwiched macrocyclic monolanthanide single-molecule magnet: The key role of axiality. *Chem.-Eur. J.* **17**, 4362–4365 (2011).
18. Guo, Y.-N. *et al.* Strong axiality and Ising exchange interaction suppress zero-field tunneling of magnetization of asymmetric Dy_2 single-molecule magnet. *J. Am. Chem Soc.* **133**, 11948–11951 (2011).
19. Lin, P.-H. *et al.* A rare μ_4-O centred Dy_4 tetrahedron with coordination-induced local chirality and single-molecule magnet behaviour. *Eur. J. Inorg. Chem.* 1535–1539 (2011).
20. Long, J. *et al.* Single-molecule magnet behavior for an antiferromagnetically superexchange-coupled dinuclear dysprosium(III) complex. *J. Am. Chem Soc.* **133**, 5319–5328 (2011).
21. Ungur, L. & Chibotaru, L. F. Magnetic anisotropy in the excited states of low symmetry lanthanide complexes. *Phys. Chem. Chem. Phys.* **13**, 20086–20090 (2011).
22. Tuna, F. *et al.* A high anisotropy barrier in a sulfur-bridged organodysprosium single-molecule magnet. *Angew. Chem. Int. Ed.* **51**, 6976–6980 (2012).
23. Rinehart, J. D. & Long, J. R. Exploiting single-ion anisotropy in the design of f-element single-molecule magnets. *Chem. Sci.* **2**, 2078–2085 (2011).
24. Gatteschi, D. & Sessoli, R. Quantum tunneling of magnetization and related phenomena in molecular materials. *Angew. Chem. Int. Ed.* **42**, 268–297 (2003).
25. Gao, W. & Cui, D. Highly cis-1,4 selective polymerization of dienes with homogeneous Ziegler–Natta catalysts based on NCN-pincer rare earth metal dichloride precursors. *J. Am. Chem Soc.* **130**, 4984–4991 (2008).
26. Jiang, S.-D. *et al.* Series of lanthanide organometallic single-ion magnets. *Inorg. Chem.* **51**, 3079–3087 (2012).
27. Jeletic, M. *et al.* An organometallic sandwich lanthanide single-ion magnet with an unusual multiple relaxation mechanism. *J. Am. Chem Soc.* **133**, 19286–19289 (2011).
28. Jiang, S.-D., Wang, B.-W., Sun, H.-L., Wang, Z.-M. & Gao, S. An organometallic single-ion magnet. *J. Am. Chem Soc.* **133**, 4730–4733 (2011).
29. Layfield, R. A. *et al.* Influence of the N-bridging ligand on magnetic relaxation in an organometallic dysprosium single-molecule magnet. *Chem.-Eur. J.* **16**, 4442–4446 (2010).
30. Sulway, S. A., Layfield, R. A., Tuna, F., Wernsdorfer, W. & Winpenny, R. E. P. Single-molecule magnetism in cyclopentadienyl-dysprosium chlorides. *Chem. Commun.* **48**, 1508–1510 (2012).
31. Ritter, S. Single-molecule magnets evolve. *Chem. Eng. News* **89**, 8–8 (2011).
32. Ishikawa, N., Sugita, M., Ishikawa, T., Koshihara, S.-y. & Kaizu, Y. Mononuclear lanthanide complexes with a long magnetization relaxation time at high temperatures: A new category of magnets at the single-molecular level. *J. Phys. Chem. B* **108**, 11265–11271 (2004).
33. Magnani, N. *et al.* Magnetic memory effect in a transuranic mononuclear complex. *Angew. Chem. Int. Ed.* **50**, 1696–1698 (2011).
34. Blagg, R. J. *et al.* Magnetic relaxation pathways in lanthanide single-molecule magnets. *Nat. Chem.* **5**, 673–678 (2013).
35. *Theory and Applications of Molecular Paramagnetism.* (Boudreaux, E. A. and Mulay, L. N. John Wiley & Sons, 1976).
36. Granroth, G. E., Vandergriff, D. H. & Nagler, S. E. SEQUOIA: A fine resolution chopper spectrometer at the SNS. *Physica B* **385–86**, 1104–1106 (2006).
37. Granroth, G. E. *et al.* SEQUOIA: A newly operating chopper spectrometer at the SNS. *J. Phys: Conf. Ser.* **251**, 012058 (2010).
38. Aquilante, F. *et al.* Software news and update MOLCAS 7: The next generation. *J. Comput. Chem.* **31**, 224–247 (2010).
39. Roos, B. O., Lindh, R., Malmqvist, P.-Å., Veryazov, V. & Widmark, P.-O. New relativistic ANO basis sets for transition metal atoms. *J. Phys. Chem. A* **109**, 6575–6579 (2005).
40. Roos, B. O., Taylor, P. R. & Siegbahn, P. E. M. A complete active space SCF method (CASSCF) using a density matrix formulated super-CI approach. *Chem, Phys.* **48**, 157–173 (1980).
41. Roos, B. O. & Malmqvist, P. Å. Relativistic quantum chemistry: the multiconfigurational approach. *Phys. Chem. Chem. Phys.* **6**, 2919–2927 (2004).
42. Ungur, L. & Chibotaru, L. F. SINGLE_ANISO program in MOLCAS (http://molcas.org/documentation/manual/node95.html).
43. Stevens, K. W. H. Matrix Elements and Operator Equivalents Connected with the Magnetic Properties of Rare Earth Ions. *Proc. Phys. Soc. A* **65**, 209 (1952).

Acknowledgments

This work was supported by the National Natural Science Foundation of China (21221061, 21301136, 21371166 and 21331003). Work at the ORNL Spallation Neutron Source is supported by the US Department of Energy Basic Energy Sciences Scientific User Facilities Division. L.U. is a postdoc of the FWO–Vlaanderen (Flemish Science Foundation). INPAC and Methusalem projects of the KU Leuven are also gratefully acknowledged. We also thank Dr. Yupeng Pan, Dr. Yang Wang and Dr. Wei Zhao for the help in preparation of sample and fruitful discussions.

Author contributions

J.T. designed and supervised the research. C.W. and D.C. carried out the synthesis and characterization studies. Y.-N.G. and J.T. planned and executed the magnetic measurements and analysed the resulting data. G.E.G. and S.E.N. performed the INS measurements. L.U. and L.F.C. performed the *ab initio* calculations and proposed the interpretation. Y.-N.G., J.T. and A.K.P. wrote the manuscript, with contributions from all the co-authors.

Additional information

Supplementary information accompanies this paper at http://www.nature.com/scientificreports

Competing financial interests: The authors declare no competing financial interests.

How to cite this article: Guo, Y.-N. *et al.* An NCN-pincer ligand dysprosium single-ion magnet showing magnetic relaxation *via* the second excited state. *Sci. Rep.* **4**, 5471; DOI:10.1038/srep05471 (2014).